0026-895X/08/7302-525–538$20.00
MOLECULAR PHARMACOLOGY
Vol. 73, No. 2
40964/3297234
Mol Pharmacol 73:525–538, 2008
Printed in U.S.A.

Multiple Binding Sites for Substrates and Modulators of Semicarbazide-Sensitive Amine Oxidases: Kinetic Consequences[S]

Andrew Holt, David J. Smith, Laura Cendron, Giuseppe Zanotti, Adelio Rigo, and Maria Luisa Di Paolo

Department of Pharmacology, Faculty of Medicine and Dentistry, University of Alberta, Edmonton, Alberta, Canada (A.H.); BioTie Therapies Corp., Turku, Finland (D.J.S.); Department of Chemistry, University of Padua and Instituto di Chimica Biomoleculare-Consiglio Nazionale delle Ricerche, Section of Padua, Padua, Italy (G.Z., L.C.); and Department of Biological Chemistry, University of Padua, Padua, Italy (A.R., M.L.D.P.)

Received August 15, 2007; accepted November 7, 2007

ABSTRACT

Human semicarbazide-sensitive amine oxidase (SSAO) is a target for novel anti-inflammatory drugs that inhibit enzymatic activity. However, progress in developing such drugs has been hampered by an incomplete understanding of mechanisms involved in substrate turnover. We report here results of a comparative study of human and bovine SSAO enzymes that reveal binding of substrates and other ligands to at least two (human) and up to four (bovine) distinct sites on enzyme monomers. Anaerobic spectroscopy reveals binding of substrates (spermidine and benzylamine) and of an imidazoline site ligand (clonidine) to the reduced active site of bovine SSAO, whereas interactions with oxidized enzyme are evident in kinetic assays and crystallization studies. Radioligand binding experiments with [^{3}H]tetraphenylphosphonium, an inhibitor of bovine SSAO that binds to an anionic cavity outside the active site, reveal competition with spermidine, benzylamine, and clonidine, indicating that these ligands also bind to this second anionic region. Kinetic models of bovine SSAO are consistent with one spermidine molecule straddling the active and secondary sites on both oxidized and reduced enzyme, whereas these sites are occupied by two individual molecules of smaller substrates such as benzylamine. Clonidine and other imidazoline site ligands enhance or inhibit activity as a result of differing affinities for both sites on oxidized and reduced enzyme. In contrast, although analyses of kinetic data obtained with human SSAO are also consistent with ligands binding to oxidized and reduced enzyme, we observed no apparent requirement for substrate or modulator binding to any secondary site to model enzyme behavior.

Human semicarbazide-sensitive amine oxidase (EC 1.4.3.6; hSSAO) is a glycosylated dimeric copper-containing enzyme found predominantly as a vascular ectoenzyme anchored to outer membranes of smooth muscle and endothelium, and also adipocytes (Boomsma et al., 2005). The extracellular portion of hSSAO is cleaved to generate a soluble enzyme that circulates in the plasma (Schwelberger, 2007). Oxidation of circulating amines such as methylamine (MA) or aminoacetone, or protein-bound amines (Lyles, 1995), likely occurs by a ping-pong mechanism, similar to that followed by other copper-containing amine oxidases (Mure et al., 2002): $E_{ox} + RCH_2NH_3^+ + H_2O \rightleftarrows E_{ox}\text{-}NH^+CH_2R \rightarrow E_{red} + RCHO + H_2O$ and $E_{red} + O_2 \rightarrow E_{ox} + H_2O_2 + NH_4^+$.

MA oxidation products such as formaldehyde and H_2O_2 contribute to vascular wall damage observed in conditions such as atherosclerosis and diabetes (Gubisne-Haberle et al., 2004). Accordingly, interest has existed for some time regarding potential therapeutic benefits of hSSAO inhibition; this

Financial support for this work was from Canadian Institutes of Health Research Operating Grant MOP77529 (to A.H.), the Faculty of Medicine and Dentistry, University of Alberta, New Faculty Establishment Grant N031000322 (to A.H.), the Consorzio "Istituto Nazionale Biostrutture e Biosistemi" (to A.R.), and the Italian Ministero dell'Istruzione e dell'Università e della Ricerca (to G.Z. and M.L.D.P.). Some of the data presented here have been presented previously at the 12th Amine Oxidase and Trace Amines Workshop (30 July–2 August 2006, Rotterdam, Holland) and at the annual meeting of the Western Pharmacology Society (4–8 March 2007, Banff, AB, Canada).

Article, publication date, and citation information can be found at http://molpharm.aspetjournals.org.

doi:10.1124/mol.107.040964.

[S] The online version of this article (available at http://molpharm.aspetjournals.org) contains supplemental material.

ABBREVIATIONS: hSSAO, human semicarbazide-sensitive amine oxidase; MA, methylamine; BPAO, bovine plasma amine oxidase; SPD, spermidine; TPQ, topaquinone; TPP^+, tetraphenylphosphonium; BZ, benzylamine; PEA, 2-phenylethylamine; CLON, clonidine; GBZ, guanabenz; (+)TCP, (+)tranylcypromine; 2-BFI, 2-(2-benzofuranyl)-2-imidazoline; (+)AM, (+)-amphetamine; PUS, partial uncompetitive inhibition by substrate.

interest has intensified with the observation that hSSAO on vascular endothelium acts as an adhesion molecule, termed vascular adhesion protein-1, which is up-regulated in some inflammatory conditions and initiates rolling of lymphocytes (Salmi and Jalkanen, 2001). Inhibitors of hSSAO activity attenuate adhesion molecule expression and lymphocyte-endothelium interactions; thus, they possess anti-inflammatory efficacy (Wang et al., 2006; Jalkanen et al., 2007).

Development of novel hSSAO inhibitors for the purposes of model and target validation and lead compound generation would be facilitated by a more complete understanding of the mechanisms by which substrates interact with hSSAO. Although molecular mechanisms have not been studied thoroughly, other closely related copper-containing amine oxidases such as bovine plasma amine oxidase (BPAO) have been characterized extensively in mechanistic and kinetic experiments (Hartmann et al., 1993; Su and Klinman, 1998; Mure et al., 2002). Nevertheless, some puzzling observations remain to be explained satisfactorily. For example, the theory that allosteric communication between monomers may occur (Morpurgo et al., 1992) is consistent with several reports documenting a reduction in initial velocity observed at higher concentrations of some substrates (Ignesti, 2003; Shepard and Dooley, 2006; Holt et al., 2007). However, the ping-pong nature of substrate oxidation by hSSAO and BPAO raises the possibility that substrates may bind to both oxidized and reduced enzyme forms, yielding hormetic kinetic plots, and recent kinetic analyses provide indirect evidence consistent with this possibility (Holt et al., 2007). Data from our laboratory also reveal an ability of several imidazoline binding site ligands to cause partial inhibition, or activation, of BPAO activity (Holt et al., 2004). Kinetic modeling implicated the involvement of up to four distinct sites through which these ligands exert their effects, although neither the locations of the putative sites nor their functional interrelationships could be deduced from the models.

The N1 and N10 atoms of the polyamine BPAO substrate spermidine (SPD) interact electrostatically with BPAO via negatively charged residues close to the topaquinone (TPQ) cofactor and in a secondary anionic cavity close to $Asp_{445'}$, on a hairpin loop extending from the opposing monomer, approximately 10 Å from TPQ (Di Paolo et al., 2003). Tetraphenylphosphonium (TPP^+), an inhibitor too large to access the BPAO active site, is able to inhibit oxidation of both SPD and benzylamine (BZ) through binding to this secondary site (Di Paolo et al., 2004). Although polyamines are not hSSAO substrates, hSSAO also possesses a similar cavity, in a similar position to that on BPAO (Airenne et al., 2005), although the cavity seems smaller and more occluded than in BPAO.

In light of data supporting substrate binding to oxidized and reduced enzymes (Holt et al., 2007) and of the affinity of the N10 primary amine group of SPD for the secondary site on BPAO (Di Paolo et al., 2003), we hypothesized that substrates and modulators of BPAO may bind to the active and/or secondary sites on both oxidized and reduced BPAO and that hSSAO may present similar targets. Direct spectroscopic evidence was obtained revealing binding of substrates and modulators to reduced BPAO, whereas radioisotopic experiments confirmed binding of ligands to both active and secondary sites. Crystallization studies revealed the manner of clonidine binding and also major structural changes induced in the enzyme-inhibitor complex. Consequences of these interactions were modeled kinetically, with derived equations allowing successful curve fitting to data showing substrate inhibition and regulation by imidazoline ligands. Kinetic analyses of hSSAO did not reveal a parallel involvement of the secondary (imidazoline) site in ligand binding, although compounds bridging the active and imidazoline sites may offer enhanced potency and selectivity as hSSAO inhibitors.

Materials and Methods

Enzyme Preparation. BPAO was purified as described previously (Di Paolo et al., 2007). The enzyme was stored at −80°C, at a concentration of approximately 8 mg/ml in 10 mM HEPES and 100 mM NaCl, pH 7.2. Full-length recombinant hSSAO was expressed in Chinese hamster ovary cells, and it was purified as described previously (Airenne et al., 2005). The enzyme was stored at 4°C, at a concentration of approximately 120 μg/ml in 20 mM phosphate-buffered saline, pH 7.4, containing Triton X-100 [0.1% (v/v)].

Assay of Enzyme Activities. The assay buffer used in all kinetic analyses was a modified Tyrode's solution buffered with HEPES (Holt et al., 2007). HEPES was dissolved in pure water (Milli-Q; Millipore Corporation, Billerica, MA) to a concentration of 100 mM. The following salts were then added to the HEPES solution to yield the indicated concentrations: 10 mM KCl, 4 mM $CaCl_2$, and 2.8 mM $MgCl_2$. The pH of the buffer was adjusted to 7.4 with NaOH (approximately 40 mM) and then NaCl was added such that the final sodium concentration in the buffer was 280 mM. After 2-fold dilution in assay wells, the concentrations of buffer components were thus half of those indicated above.

Three distinct approaches were used to measure initial rates of amine oxidation by SSAO enzymes. Most kinetic assays were done following one of two alternative continuous peroxidase-coupled plate reader-based protocols. A fluorescence protocol, with Amplex Red as fluorogen (Holt et al., 2007), or an absorbance protocol, generating a quinoneimine dye from 4-aminoantipyrene and 2,4-dichlorophenol (Holt and Palcic, 2006), was done as described previously. In brief, fluorescence assays were made in black polystyrene 96-well plates (Whatman, Maidstone, UK), in a volume of 200 μl, containing amine substrate (50 μl in water) or water in blank wells, Amplex Red (50 μl in modified Tyrode-HEPES buffer containing 4 U/ml type II horseradish peroxidase, to give a final assay concentration of Amplex Red of 20 μM), test compound (50 μl in water), or water in control and blank assay wells, and the reaction was started by the addition of enzyme (50 μl in modified Tyrode-HEPES buffer). The increase in fluorescence associated with generation of resorufin was monitored in a SpectraMax Gemini XPS plate reader (λ_{ex}, 560 nm; λ_{em}, 591 nm; cut-off filter, 590 nm). Absorbance assays were made in clear polystyrene 96-well flat-bottomed plates (Corning Inc., Corning, NY), in a volume of 300 μl, containing amine substrate (75 μl in water) or water in blank wells, 75 μl of chromogenic solution (containing 4 U/ml type II horseradish peroxidase, 500 μM 4-aminoantipyrine, and 1 mM 2,4-dichlorophenol in modified Tyrode-HEPES buffer), test compound (75 μl in water), or water in control and blank assay wells, and the reaction was started by the addition of enzyme (75 μl in modified Tyrode-HEPES buffer). The increase in absorbance associated with generation of the quinoneimine dye was monitored in a SpectraMax 190 plate reader (λ_{abs} 510 nm). All kinetic assays were done at 30 or 37°C, with three to six replicates per experiment, and initial rates were obtained from product versus time data with the linear regression facility of SoftMax Pro version 4.8 (Molecular Devices, Sunnyvale, CA).

Substrates used in kinetic assays were, with BPAO, SPD and BZ, and with hSSAO, MA, BZ, and 2-phenylethylamine (PEA) (Holt et al., 2007). The reversible compounds assessed as modifiers of enzyme activity are shown in Fig. 1. For BPAO, they were TPP^+ (Di Paolo et

al., 2004), clonidine (CLON) (Holt et al., 2004), guanabenz (GBZ) (Ozaita et al., 1997; Holt et al., 2004), (+)-tranylcypromine [(+)TCP)] (Carpéné et al., 1995), and 2-(2-benzofuranyl)-2-imidazoline (2-BFI) (Holt et al., 2004); and for hSSAO, they were (+)TCP, GBZ, and (+)-amphetamine [(+)AM] (Lyles, 1984). Although fluorescence quenching or inhibition of peroxidase have been observed with several amine oxidase substrates and inhibitors (Sayre et al., 1996; Holt and Palcic, 2006), preliminary screening assays confirmed that none of the modulators used interfered with chromogenic or fluorogenic reagents. Modifier ligands were shown in a dilution assay to bind reversibly to the enzymes (data not shown), with reversibility being an important requirement of the kinetic analytical approach adopted.

Kinetic Model Development. Based on observations from previous kinetic experiments (Holt et al., 2007), reaction schemes were drawn that might account for the ligand-enzyme interactions observed, and corresponding rate equations were then formulated. These were entered as user-defined equations within the nonlinear regression facility of GraphPad Prism version 5.00 (GraphPad Software Inc., San Diego, CA). Equations were applied to multiple data sets, composed of several v versus [S] curves generated at different inhibitor/modulator concentrations, with the global curve-fitting facility of Prism allowing data from all curves to contribute to generation of universal kinetic constants. A consistently good fit (usually $r^2 > 0.90$ for every data set) obtained by global curve fitting, with no obvious pattern of digression of fitted curves from data points, was viewed as supportive of the proposed model. A failure in this regard resulted in the scheme being considered inconsistent with the observed results.

Previous observations have suggested that substrates may bind to two sites on each SSAO monomer (either BPAO or hSSAO), with the most likely explanation being that amines bind to the active site in both oxidized and reduced forms of SSAO enzymes (Holt et al., 2007). In addition, a second site within the substrate entrance channel of BPAO has been identified, to which inhibitors such as TPP^+ and the amine group at the 10-position of spermidine likely bind (Di Paolo et al., 2003, 2004). The reaction schemes developed thus allowed for the possible interactions of substrates and inhibitors with one or both of the active and secondary sites, on both the oxidized and reduced forms of the enzymes.

The method used to generate equations from reaction schemes was a "pseudoquantitative" rapid equilibrium approach, developed recently in our laboratory (Holt et al., 2007). The nonsequential (ping-pong) nature of the SSAO reaction, with the existence of enzyme in both oxidized and reduced forms, precludes rapid equilibrium analyses and demands that a steady-state approach be used (Segel, 1993). However, the complexity of the proposed models, coupled with a lack of suitable software to facilitate equation derivation, demanded that an alternative means of generating equations be found. To permit use of a rapid equilibrium approach, reaction schemes were drawn in which "ES" refers both to the complex between oxidized SSAO and substrate, and to the reduced enzyme after release of aldehyde. Thus, "ESS" refers to a complex between a single substrate molecule and reduced enzyme; the apparent presence of a single enzyme species (E) allows derivation of equations by a rapid equilibrium approach (Segel, 1993). Theoretical modeling studies indicate that although this pseudoquantitative approach generates equations yielding dissociation and rate constants that differ to varying degrees from true values, global curve fitting to multiple data sets nevertheless provides a valid indication of whether a proposed reaction scheme might explain experimental kinetic data obtained (Holt et al., 2007).

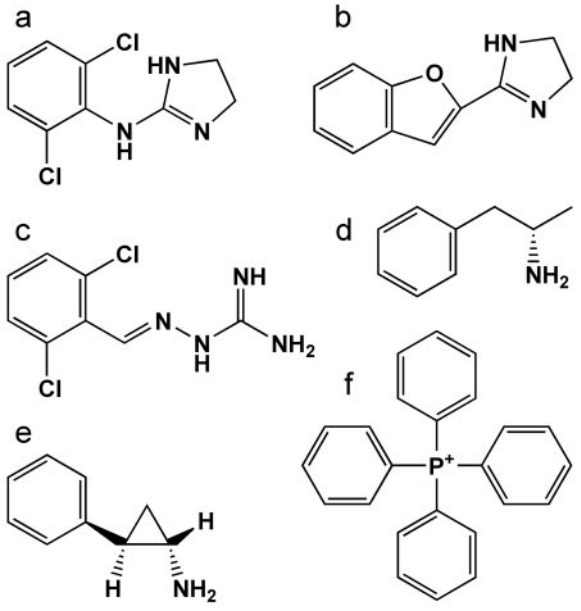

Fig. 1. Structures of SSAO ligands used in these studies. Clonidine (a), 2-BFI (b), guanabenz (c), *S*-(+)-amphetamine (d), 1*S*,2*R*-(+)-tranylcypromine (e), and tetraphenylphosphonium (f).

Radioligand Binding. To assess directly the binding characteristics of the interaction between TPP^+ and BPAO, and to determine whether substrates and inhibitors might compete with TPP^+ for binding to the imidazoline site on BPAO, a novel radioligand binding procedure was devised. Preliminary experiments (data not shown) indicated that BPAO was not retained on a Whatman GF/B fiberglass filter, whereas nonspecific binding of TPP^+ to filters, and to plastics such as pipette tips, resulted in reduced ligand concentration and very high background counts. Therefore, we adapted a method used previously for quantifying binding of $^{45}Ca^{2+}$ to proteins (Menguy et al., 1998).

In experiments to determine binding constants for TPP^+, BPAO (250 μl; ≈40 nM in modified Tyrode-HEPES buffer), [^{3}H]TPP^+ (100 μl; nominally 0.5 nCi/pmol: prepared at initial concentrations of 0.25–8.75 μM), 10 mM TPP^+ (50 μl, to define nonspecific binding) or water (50 μl to define total binding), and water (100 μl), were pipetted into the sample reservoir of a Microcon YM-10 centrifugal filter device (molecular mass cut-off 10 kDa; Millipore Corporation). Therefore, each reservoir contained ≈20 pmol of BPAO subunits. The concentration of BPAO subunits was determined accurately by titrating an aliquot of BPAO solution with *p*-nitrophenylhydrazine and monitoring both the absorbance increase at 455 nm as a result of formation of TPQ-nitrophenylhydrazone adduct and the corresponding loss of enzymatic activity (Holt et al., 1998). Samples were incubated at 30°C for 15 min before centrifugation (25°C; 14,000*g*) for 40 min. Centrifugation resulted in removal of more than 99% of unbound [^{3}H]TPP^+, without reducing the ligand concentration and thus without altering the proportion of BPAO bound by ligand. The sample reservoir containing the BPAO-[^{3}H]TPP^+ complex was detached from the filtrate vial, and the entire reservoir was placed in a 6-ml plastic scintillation vial with EcoLite(+) scintillation fluid (4 ml; MP Biomedicals, Solon, OH) and was allowed to soak for 18 h before counting for 5 min in an LS6500 liquid scintillation counter (Beckman Coulter, Fullerton, CA).

To account for ligand depletion due to the high affinity of [^{3}H]TPP^+ for plastics and also due to binding to BPAO in assays where low concentrations of TPP^+ were not in significant excess over that of BPAO, the concentration of unbound TPP^+ at equilibrium was determined experimentally. An aliquant of the filtrate from each assay (100 μl) was counted for radioactivity in 2 ml of EcoLite(+) (V1). The remaining solution in each filtrate vial was transferred to a second scintillation vial (V2), and it was counted for radioactivity as described above. To a third scintillation vial (V3), we added the empty filtrate vial, along with the pipette tip used to transfer samples of retentate to vials 1 and 2, and the contents were counted for radioactivity in 4 ml of EcoLite(+), after vigorous shaking and soaking for 18 h. The free ligand concentration at equilibrium, which was assumed to be equal to the free

ligand concentration in the filtrate after centrifugation, was calculated from eq. 1:

$$[TPP^+]_{free}\ (\mu M) = \frac{n(nmol)}{volume\ (ml)} = \frac{\left(\frac{V1dpm + V2dpm + V3dpm}{specific\ activity\ (dpm/nmol)}\right)}{\left(\frac{V1dpm + V2dpm + V3dpm}{V1dpm}\right) \times 0.1\ ml} \quad (1)$$

where V1dpm, V2dpm, and V3dpm refer to the measured radioactivity in scintillation vials V1, V2, and V3, respectively.

[^{3}H]TPP$^+$ was prepared at the desired concentrations in silanized microcentrifuge tubes, by diluting a stock solution of [^{3}H]TPP$^+$ (nominally 0.5 nCi pmol^{-1}) with water. The actual specific activity of this stock solution was determined directly by counting an aliquot of the solution, along with the pipette tip used to remove the aliquot, in 3 ml of EcoLite(+), because a portion of the ligand in the high-activity manufacturer's stock solution was lost through binding to the pipette tip used to remove the initial small volume from the manufacturer's stock vial. Standard curves prepared thereafter from all prepared [^{3}H]TPP$^+$ solutions were linear ($r^2 > 0.999$), but they crossed the abscissa below zero (data not shown), suggesting a consistent amount of [^{3}H]TPP$^+$ lost to binding to plastic from all samples, even when silanized plasticware was used.

Specific binding was calculated as (total binding − nonspecific binding) and was plotted versus calculated concentrations for free [^{3}H]TPP$^+$. Hyperbolic curves were fitted to data with the nonlinear regression facility of GraphPad Prism.

In competition binding experiments to assess the abilities of other SSAO ligands to compete with TPP$^+$ for binding to the imidazoline site, binding experiments were done as described above, but in the presence of a single concentration of [^{3}H]TPP$^+$ (nominally 150 nM; 0.5 nCi pmol^{-1} in the assay) and with water (100 μl) replaced by 100 μl of the competing ligand, dissolved in water. Ligands examined were TPP$^+$ (30 nM–10 μM), BZ (1–300 mM), SPD (100 μM–30 mM), and CLON (30 μM–10 mM). The specific activity and free concentration of [^{3}H]TPP$^+$ were determined as described above. Specific binding, expressed as a percentage of that in control experiments in which competitive ligands were replaced by water, was plotted versus $\log_{10}$[competitor], and sigmoidal curves were fitted with the nonlinear regression facility of GraphPad Prism.

Anaerobic Spectroscopy. Benzylamine-induced reduction of BPAO was achieved after a modification of published procedures (Hartmann et al., 1993; Shepard and Dooley, 2006). High-purity argon (grade 5; ≥99.9997%; Matheson Tri-Gas, Newark, CA) was passed through a PUR-Gas oxygen purifier (Matheson Tri-Gas) and was then bubbled through pure water in a sealed plastic conical tube to hydrate the gas. An argon flow rate of approximately 8 ml/min was maintained. The copper line carrying oxygen-free hydrated argon from the conical tube was spliced to supply both the sample preparation cuvette and the cuvette chamber of a DU640 spectrophotometer (Beckman Coulter). The line carrying the argon to the spectrophotometer entered the cuvette chamber via an access port normally used for circulating warm water to regulate cuvette temperature, and complete exclusion of light was thus maintained.

Modified Tyrode-HEPES buffer was degassed under house vacuum, and it was then bubbled overnight with hydrated argon, in a sealed plastic conical tube with a PTFE/silicone septum glued over an access hole drilled in the plastic lid. This oxygen-free buffer was used in all subsequent anaerobic studies. BPAO was prepared at 10.3 μM in oxygen-free buffer containing 50 U/ml catalase and 30 mM D-glucose in a sealed septum-cap vial flushed with argon. The solution was then flushed gently with hydrated argon via a 25-gauge 5/8-in. needle inserted through the PTFE/silicone septum, with a second needle allowing argon to exit the cuvette. After flushing for 90 min on ice, the vial was allowed to warm to 22°C, and 20 μl of glucose oxidase was added to the vial contents via injection with a gas-tight syringe, to yield a glucose oxidase concentration of 50 U/ml. The vial was flushed for a further 30 min with hydrated argon and was then replaced on ice. An aliquant of this solution (390 μl) was injected through a septum into an argon-flushed 0.6-ml quartz (far-UV) glass anaerobic cuvette (pathlength 1 cm; Spectrocell, Oreland, PA) with a gastight syringe. The cuvette was placed in the spectrophotometer, and the contents were flushed gently with hydrated argon via a needle penetrating the septum, as described above, for a further 5 min. This steady flow of argon into the anaerobic cuvette was maintained for the duration of the experiments, ensuring no slow leakage of air into the cuvette. A blank spectrum (240–700 nm) was then measured for this solution. A solution of BZ (2 mM) was prepared in oxygen-free buffer in a sealed septum-cap vial flushed with argon, and 10 μl was injected with a gas-tight syringe into the cuvette containing BPAO. The BZ concentration (50 μM) was thus 5 times that of the BPAO present (10 μM). After rapid mixing with a second gas-tight syringe primed with argon, reduction of BPAO was observed by obtaining difference spectra (240–700 nm) at several time points after injection of BZ, until spectra remained stable. At this point, a blank spectrum was again obtained for the cuvette contents.

Solutions of BZ (800 mM), SPD (16 mM), and CLON (3.2 mM) were prepared in oxygen-free buffer, and they were flushed with argon in sealed septum-cap vials. To assess whether these ligands interact with the active site of reduced BPAO, ligands were injected cumulatively into the anaerobic cuvette with a gas-tight syringe, in volumes of 2.5, 5, or 10 μl, to generate a range of concentrations of the ligands. Difference spectra (240–700 nm) were obtained at several time points after each injection, until spectra remained stable. A fresh preparation of reduced BPAO was used to examine each of the three ligands of interest. Corrections were made to measured absorbance values to account for enzyme dilution on addition of ligands.

TPP$^+$ chloride (2.5 mM) was prepared in oxygen-free buffer, and it was flushed with argon in a sealed septum-cap vial. To determine the degree to which ligands binding to the imidazoline site influenced the spectra obtained for reduced cofactor, 10 μl of this solution was injected after the final ligand aliquant had been added to the anaerobic cuvette and spectra had stabilized. The resulting concentration of TPP$^+$ (≈50 μM) was sufficiently high to displace other ligands binding to the imidazoline site. Difference spectra (240–700 nm) were obtained at several time points after addition of TPP$^+$, until spectra remained stable.

Spectral data from all scans were captured and transferred to GraphPad Prism, and absorbance readings were then corrected by applying the Beer-Lambert equation to account for protein dilution on addition of ligand, before data were plotted.

Crystallography Studies of the BPAO-Clonidine Complex. BPAO was crystallized as reported previously (Calderone et al., 2003). In brief, after purification, the enzyme was deglycosylated with a glycoprotein deglycosylation kit (Calbiochem, San Diego, CA), dialyzed in 10 mM HEPES, pH 7.2, containing 10 mM NaCl, and concentrated to 2 to 2.4 mg/ml. The BPAO sample was incubated in the presence of 2 mM CLON at 25°C for 2 h. Thereafter, crystals were grown by the vapor-diffusion technique at 25°C, by mixing equivalent volumes of the BPAO-CLON sample and a standard precipitant solution containing 0.2 M KH_2PO_4, pH 7.4, and polyethylene glycol 3350 [20% (w/v)], and the enzyme was left to equilibrate against the precipitant. The crystals grew within 3 weeks.

The X-ray data were collected at the BM16 beamline of the European Synchrotron Radiation Facility (Grenoble, France). The crystals were mounted directly under a nitrogen flux (−173°C), without addition of cryoprotectant. The data were processed using the MOSFLM program (Leslie, 1992). Crystals seemed isomorphous to the apoenzyme structure (Protein Data Bank code 1TU5) determined previously (Lunelli et al., 2005). One dimer, corresponding to an independent biological unit, was present in the asymmetric unit (Supplemental Table S1). The structure of the apoenzyme (1TU5) was used as the starting model, including the TPQ_{470}-modified ty-

rosine residue. After several cycles of rigid body and restrained refinement with Refmac software (Murshudov et al., 1997), the two copper cations bound within the active sites could be identified. Some residual electron density in the same pocket was also observed, which could be attributed only to the CLON molecules bound to the enzyme. In particular, the two chloride atoms of each CLON molecule were visible in the Fourier difference map at more than 3 σ. Both active sites seemed similar in this regard, with minor differences likely attributable to incomplete occupancy of the active sites by CLON, because of the low affinity of CLON for that site.

The inhibitor molecule was constructed with PRODRG software (Schüttelkopf and van Aalten, 2004), and it was aligned to fit within the residual electron density. Noncrystallographic symmetries were introduced to account for the binary axis relating the two molecules of the dimer present in the asymmetric unit. However, all the residues belonging to the active site cavity and the more flexible regions were excluded. In further refinement steps (Murshudov et al., 1997; Sheldrick and Schneider, 1997), 342 water molecules were added to the structure, resulting in a final R-factor of 23.7% and an R-free of 25.2%. Data processing and refinement statistics are shown in Supplemental Table S1.

Coordinates have been deposited at the Protein Data Bank of the Research Collaboratory for Structural Bioinformatics (http://www.rcsb.org/pdb) with accession number 2PNC.

Materials. [Phenyl-^{3}H]tetraphenylphosphonium bromide (29.0 Ci mmol^{-1}; 1.0 mCi/ml) was purchased from Moravek Biochemicals (Brea, CA). Tetraphenylphosphonium chloride, methyltriphenylphosphonium iodide, dimethyldiphenylphosphonium iodide, trimethylphenylphosphonium iodide, clonidine hydrochloride, guanabenz, catalase, glucose oxidase, horseradish peroxidase (type II), 4-aminoantipyrene, 2,4-dichlorophenol, and amine substrates (as their hydrochloride salts) were from Sigma-Aldrich (Oakville, ON, Canada). Amplex Red was obtained from Invitrogen (Burlington, ON, Canada). 2-BFI was purchased from Tocris Cookson Inc. (Ellisville, MO). (+)- and (−)-TCP and (+)-amphetamine were generous gifts from Dr. Glen Baker (University of Alberta, Edmonton, AB, Canada). All other materials were of molecular biology grade, and they were purchased from Fluka-Sigma-Aldrich or EMD Biosciences/Calbiochem (San Diego, CA).

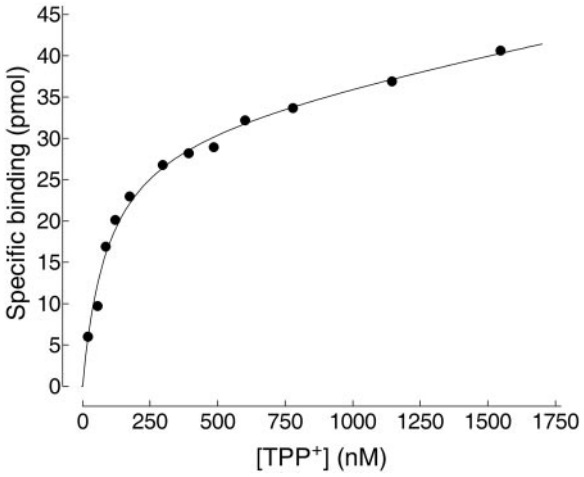

Fig. 2. Specific binding of [^{3}H]TPP$^+$ to BPAO. To quantify total binding, BPAO (17.4-pmol subunits) and [^{3}H]TPP$^+$ were added to the sample reservoir of a Microcon YM-10 centrifugal filter device. After incubation (15 min at 30°C), devices were centrifuged to remove >99% of unbound [^{3}H]TPP$^+$, and reservoirs were then soaked in scintillation fluid and were counted for radioactivity. Nonspecific binding was quantified in parallel experiments by including 1 mM TPP$^+$ in the reservoirs. Calculated values for specific binding (total binding minus nonspecific binding) were plotted, and data fitted by nonlinear regression to an equation for two-site hyperbolic binding. The high-affinity B_{max} of 32 pmol per 17.4-pmol subunits indicates binding of two [^{3}H]TPP$^+$ molecules to two high-affinity sites per subunit, with similar K_d values of around 94 nM. Replicate readings were not made, because final free ligand concentrations could only be determined after centrifugation.

Results

Binding of [^{3}H]TPP$^+$ to BPAO. Fig. 2 shows specific binding of [^{3}H]TPP$^+$ to 17.4 pmol of BPAO subunits. Nonspecific binding (data not shown) was linear and passed through the origin. Thus, the failure to reach a plateau is due to a low-affinity component of the specific binding, rather than to incomplete determination of the nonspecific contribution to total binding. Data are fitted to an equation for two-site hyperbolic binding (Prism version 5.0). Although nonlinear regression failed to yield meaningful values for K_d or B_{max} for the low-affinity component of specific binding, likely due to the low-affinity K_d lying beyond the highest TPP$^+$ concentration used in these experiments, the high-affinity component had a K_d of 94 nM and a B_{max} of 32 pmol sites per assay well. This B_{max} value is double that expected, based on the known concentration of BPAO subunits, and it indicates binding of two TPP$^+$ molecules per BPAO subunit. Although it is hypothesized that one of these sites is the secondary site within the substrate entrance channel, the location of the other site is not known, although binding to the active site can be discounted based upon kinetic observations. Nevertheless, the two sites seem to bind TPP$^+$ with similar affinities, because trihyperbolic curve fitting failed to separate two distinct high-affinity binding components without restricting some of the variables (data not shown). In this regard, an affinity of TPP$^+$ for the secondary site of around 100 nM is consistent with the inhibitor dissociation constant of around 140 to 200 nM for TPP$^+$ determined in kinetic experiments (Table 1 and Supplemental Table S2).

Competition with [^{3}H]TPP$^+$ for Binding to BPAO. The abilities of TPP$^+$, SPD, BZ, and CLON to compete with specific binding of [^{3}H]TPP$^+$ were assessed. At the concentration of [^{3}H]TPP$^+$ used (calculated at ≈106 nM), the contribution of low-affinity binding was presumed to be negligible. Figure 3 shows competition curves for ligands of interest, revealing complete inhibition of binding by TPP$^+$ but inhibition of only around 50% of binding by SPD and BZ. A two-site competition equation applied to data for TPP$^+$ failed to differentiate between two high-affinity binding sites (data not shown). CLON also failed to inhibit completely the binding of [^{3}H]TPP$^+$, although results from nonlinear regression suggested that more than 50% of binding may be inhibited and thus that CLON may also compete for binding at the second high-affinity TPP$^+$ binding site. Dissociation constants were estimated from the Cheng-Prusoff equation, making the assumptions that TPP$^+$ was present at a concentration similar to its K_d value at the secondary site and that binding of all ligands within the concentration ranges used was uniphasic. Dissociation constants thereby estimated were 234 nM (TPP$^+$), 296 μM (SPD), ≈1.2 mM (CLON), and 13.5 mM (BZ); therefore, values shared the same rank order of affinities as constants determined kinetically (K_M, K_{imid}, and K_{sec} values in Table 1 and Supplemental Table S2), although K_d values for the lower affinity ligands (CLON and BZ) differed quite significantly from constants determined kinetically. These observations confirm that a single SPD molecule probably binds both to the active site and to the secondary anionic site within the substrate entrance channel. Furthermore, small

cationic substrates and inhibitors may bind simultaneously at the active and secondary sites, with the latter action potentially influencing substrate turnover kinetics at the active site.

Under assay conditions used to assess interactions of ligands with oxidized BPAO, some oxidation of SPD and BZ would be expected during incubation with BPAO in the presence of [^{3}H]TPP$^+$, resulting in depletion of these substrates and generation of oxidation products that might influence TPP$^+$ binding in some way. Although the estimated depletion of SPD (≥12%) was rather higher than that for BZ (≥0.5%), analysis of data obtained in the presence of SPD (Fig. 3) revealed a monophasic curve with Hill slope not significantly different from unity and indicative of a K_d value similar to K_M and K_i values obtained in kinetic analyses. Thus, there is no outward indication of any unexpected effect due, for example, to interactions of SPD oxidation products with the enzyme.

The second high-affinity TPP$^+$ binding site, for which BZ and SPD do not compete, could be the secondary external cation binding site present on each subunit that was found to coordinate Ca^{2+} and other cations (Lunelli et al., 2005).

Confirmation of Substrate and Drug Binding to Reduced BPAO. After reduction of anaerobic BPAO with a 5-fold excess of BZ, further addition of SPD (99 μM–2.1 mM), BZ (5–104 mM), or CLON (78–640 μM) resulted in concentration-dependent spectral changes associated with binding of ligands to the reduced enzyme (Fig. 4), and, presumably, perturbation of the absorbance characteristics of reduced cofactor (Hartmann et al., 1993). Specifically, after consideration of the blank spectra of ligands alone (data not shown), binding of SPD resulted in the appearance of peaks at around 251 and 299 to 306 nm, BZ binding resulted in the appearance of a peak at around 297 nm, and CLON binding resulted in the appearance of peaks at around 246 and 310 nm. Because the peaks occurring in each case in the region of 297 to 310 nm may result from perturbation of species similar to that described previously as being associated with the complex between reduced BPAO and BZ (Hartmann et al., 1993), peak heights were plotted versus ligand concentrations (Supplemental Fig. S1). Based on the assumption that observed spectral changes were a result of interactions of ligands at the active site, rather than at the secondary site, data were fitted by nonlinear regression to a four-parameter logistic equation (Prism version 5.0) to estimate the affinities of ligands for the active site of the reduced enzyme. The approximations for K_d values obtained were ≈265 μM (SPD) and ≈59 mM (BZ). No point of inflection, and thus no estimate of K_d, was obtained from data from experiments with CLON. The rank order of potency of these estimates is similar to that for binding of these substrates to the active site of the reduced enzyme obtained by kinetic analyses, of around 520 μM (SPD) and around 4.21 mM (BZ). (K_i values in Table 1 and Supplemental Table S2).

Addition of TPP$^+$ (≈50 μM) to anaerobic cuvettes containing reduced BPAO and SPD, BZ, or CLON failed to reverse spectral changes caused by these ligands (data not shown). Because this concentration of TPP$^+$ should be sufficiently high to displace ligands almost completely, these observations suggest that spectral changes on addition of SPD, BZ, or CLON result predominantly from ligands binding at the BPAO active site, rather than at the secondary imidazoline site. Addition of TPP$^+$ alone to reduced BPAO induced only minor spectral differences (data not shown).

Crystal Structure of the BPAO-Clonidine Complex. The dimeric architecture and quaternary structure of the enzyme in complex with CLON are well conserved, compared with the apoenzyme (Lunelli et al., 2005). Superpositioning of Cα atoms shows an overall root mean square deviation value of 0.35 Å, with major changes involving the residues defining the catalytic pocket and the substrate entrance channel (Supplemental Table S3). Loops Tyr_{230}-His_{240} and Met_{467}-Asp_{471} exhibit the highest Cα displacements. Asn_{469} rotates approximately 180° away from the internal pocket to face the mouth of the entrance channel, thereby permitting the docking of CLON. In addition, several residues (Gly_{580}-Ala_{581}, Ala_{610}-Pro_{613} and Val_{696}-Gly_{701}) forming an internal channel present at the interface between monomers show small but significant displacements with respect to native BPAO. This channel may represent a conduit through which molecular oxygen can reach the active site and H_2O_2 could exit (Lunelli et al., 2005). Some displacement was also evident in the residues forming a hairpin loop (Val_{430}-Val_{460}), protruding from each monomer to wrap around the other subunit. In this case, the residues between His_{442} and Gly_{452} were not visible at all in the electron density maps, and some

TABLE 1

Kinetic constants determined for metabolism of SPD by BPAO in the presence of modulatory ligands, measured in an absorbance assay

Data were obtained from global nonlinear regression of five data sets (curves) composed of 18 points per curve, with five replicate determinations made for each point. Curves were fitted with the equations indicated. K_i is the equilibrium constant for binding of substrate to the active site of reduced enzyme. K_{act} and K_{imid} are equilibrium constants for binding of drug ligands to the active and imidazoline sites of oxidized enzyme, respectively. All Greek letters (including γ, δ, σ, ϵ, and π) are factors indicating the degrees to which equilibrium constants for substrates and drug ligands are altered when binding is to reduced enzyme or when binding is to an enzyme species already bound by another ligand. All lower case letters (including a, d, e, f, and g) are factors indicating the degrees to which the catalytic rate constant k_p is altered as a result of substrate combining with reduced enzyme or when product is released from an enzyme form to which an inhibitor is bound (see Schemes 1–4 and Fig. 11 for further details). Values in parentheses indicate S.E.M. from nonlinear regression analyses. (+) indicates S.E.M. significantly greater than the estimated value for the parameter in question. Data from experiments with TPP$^+$ are fitted with a modified version of eq. 2 (see text). Mean values are shown for substrate-dependent kinetic constants expected to remain unaltered in the presence of modulators.

Modulator	Eq. No.	V_{max}	K_M	K_i	K_{imid}	K_{act}	γ	δ
		mOD/min			*μM*			
Control	PUS[a]	5.56 (0.33)	40.2 (5.5)	456 (137)				
TPP$^+$	2	5.91 (0.21)	41.0 (3.6)	543 (77)	0.141 (0.018)		2.57 (0.56)	
CLON	S2	5.17 (0.30)	35.5 (5.2)	466 (163)	42.4 (+)	23.4 (+)	13.2 (+)	0.932 (+)
GBZ	S2	6.31 (0.24)	38.2 (3.8)	782 (180)	1.40 (+)	0.518 (+)	1.50 (+)	40.9 (+)
2-BFI	S2	5.55 (0.37)	36.4 (5.6)	310 (109)	8.70 (+)	118 (+)	5.07 (+)	88.5 (+)
(+)TCP	S2	6.96 (0.34)	40.8 (5.0)	565 (148)	63.5 (+)	4.56 (+)	2.90 (+)	1.097 (+)
Mean ± S.E.			38.7 ± 1.0	520 ± 64				

[a] Partial uncompetitive inhibition by substrate (see Holt et al., 2007). Control data were those obtained from experiments with modulators where [modulator] = 0.

residues just before and after that fragment show a strong displacement and high temperature factors (Supplemental Table S3). However, this region is also highly flexible in the apoenzyme structure, thereby indicating a somewhat flexible nature for this protein arm.

One molecule of CLON binds similarly in each of the two active sites of the BPAO dimer. CLON extends as far as the bottom of the funnel-shaped, solvent-accessible catalytic cavity next to TPQ_{470}. Binding of CLON causes a displacement of TPQ, inducing a rotation of the TPQ side chain to the "on-copper" nonproductive orientation, in which the hydroxyl group of TPQ coordinates the copper ion, together with three histidine residues (His_{519}, His_{521}, and His_{683}). The phenyl ring of CLON is observed to lie almost perpendicular to the imidazolidine portion of the molecule, according to the more stable conformation optimized by Remko et al. (2001), and it is clearly trapped by stacking interactions in a "sandwich-like" orientation within the aromatic side chains of TPQ_{470} and Tyr_{472} residues (Fig. 5).

Two of the nitrogen atoms (N2 and N3) in the imidazolidine moiety are at a suitable orientation and distance to interact through hydrogen bonding with Asp_{385}, the general catalytic base (Hartmann et al., 1993; Mure et al., 2002). The N3 nitrogen in the heterocyclic ring can also strengthen the inhibitor-enzyme interaction through a NH-π interaction with Tyr_{383} (Fig. 5).

Kinetic Analyses of BPAO-Ligand Interactions. With SPD as substrate, kinetic analyses of the effects of TPP^+ on BPAO activity (Fig. 6) were consistent with a model (Scheme 1) in which a single SPD molecule could bridge the active and secondary sites on a monomer, and in which TPP^+ could inhibit binding and oxidation of SPD through a competitive interaction at a single site. However, although Scheme 1 is described by eq. 2:

$$v = \frac{V_{max}[S]}{K_M\left(\frac{1+\frac{[I]}{K_{act}}}{1+\frac{a[S]}{K_i}+\frac{f[I]}{\sigma K_{act}}}\right)+[S]\left(\frac{1+\frac{[S]}{K_i}+\frac{[I]}{\sigma K_{act}}}{1+\frac{a[S]}{K_i}+\frac{f[I]}{\sigma K_{act}}}\right)} \quad (2)$$

data were fitted with a *modification* of eq. 2, in which the terms K_{act}, σ, and f were replaced with the terms K_{imid}, γ, and d, respectively, to reflect the fact that single site binding of TPP^+ occurs to the imidazoline site rather than to the active site with that particular ligand (see Table 1 for definitions of terms used). Kinetic constants were determined and are listed in Table 1. In contrast, when BZ was used as substrate, TPP^+ was significantly less potent as an inhibitor (Fig. 7), and data could be fitted with similar success to models in which BZ bound only to the active site, or to both the active and secondary sites (Scheme 2), on both oxidized and reduced enzyme, with binding of TPP^+ again restricted to the secondary site. Because radioligand binding studies had suggested that BZ binds both to the active and secondary sites, kinetic constants (Supplemental Table S2) were thus obtained after fitting of data to an appropriate equation (Supplemental eq. S1) based on scheme 2.

Although TPP^+ is too large to enter the active site cavity of BPAO, the other modulators of enzyme activity examined [CLON, GBZ, 2-BFI, and (+)TCP] are sufficiently small that access might be gained both to the active and to the secondary sites. With SPD as substrate, kinetic analyses of the effects of CLON on BPAO activity (Fig. 8) were consistent with a model (Scheme 3) in which CLON could compete with SPD binding through interactions at both the active and secondary sites, on both forms of the enzyme. This contention was supported by data from radioligand binding and crystallization studies (vide supra). Data were fitted with an appropriate equation (Supplemental eq. S2) from which kinetic constants were determined (Table 1). The effects of GBZ, 2-BFI, and (+)TCP on SPD oxidation could also be described successfully with this equation, and kinetic constants thereby derived are listed in Table 1. (−)-Tranylcypromine was largely devoid of inhibitory potency (data not shown).

When BZ was used as substrate, acceptable fits could not be obtained with equations derived from models based upon an interaction of CLON with a single site, whether for BZ interacting only with the active site, or with both the active and secondary sites. Although better fits were attainable with models requiring binding of CLON to both sites, the number of kinetic and rate constants (variables) in the associated equations (14 for BZ binding to the active site and 23) for BZ binding to the active and secondary sites, on both oxidized and reduced enzyme) made global curve fitting difficult without constraining several variables. Nevertheless, based on deductions from results of other experiments described here, the latter model (Scheme 4) and associated equation (Supplemental eq. S3) were used to fit curves to data showing effects of CLON upon BZ oxidation by BPAO (Fig. 9). Several variables were initially constrained to equal those determined in experiments with CLON in which SPD was the substrate used, to facilitate preliminary regression

σ	ϵ	π	a	d	e	f	g	r^2	n
			0.448 (0.023)					0.620	25
			0.387 (0.012)	0.00233 (0.063)				0.935	5
2.81 (+)	0.825 (+)	3.31 (+)	0.506 (0.026)	4.25 (+)	0.776 (0.165)	1.02 (+)	≈0	0.956	5
4.89 (+)	1.34 (+)	1.49 (+)	0.417 (0.020)	0.194 (+)	≈0	0.0572 (+)	≈0	0.962	5
2.70 (+)	0.316 (+)	2.05 (+)	0.528 (0.03)	1.01 (+)	≈0	1.92 (+)	≈0	0.963	5
23.9 (+)	0.795 (+)	0.291 (+)	0.458 (0.021)	0.431 (+)	≈0	0.629 (+)	≈0	0.940	5
			0.457 ± 0.022						

analyses. Calculated variables obtained thereafter are listed in Supplemental Table S2. Data from experiments with 2-BFI and GBZ were also fitted with Supplemental Eq. S3, in the manner described above (Supplemental Table S2). In contrast with CLON, which enhanced the oxidation rate of BZ significantly at all concentrations of CLON used, only inhibition of BZ oxidation was observed in the presence of GBZ, 2-BFI, or (+)TCP. Analyses of model data (data not shown) suggested that marked enhancement of substrate turnover can only occur when enzyme reoxidizes faster with drug bound to E_{red} than with substrate bound, regardless of relative affinities of the ligands for E_{ox} and E_{red}.

Although data presented here demonstrate clearly the abilities of several imidazoline binding site ligands such as CLON, 2-BFI, and GBZ to interact with BPAO and influence enzyme activity, the ligand specificity of the imidazoline site identified on BPAO, and the affinities of these ligands for this site, indicate that the present site does not display characteristics typical of other imidazoline sites identified and characterized thus far (Head and Mayorov, 2006).

Kinetic Analyses of hSSAO-Ligand Interactions. As is the case with BPAO, an anionic binding cavity can be seen at the mouth of the substrate entrance channel on an hSSAO monomer (Airenne et al., 2005). However, in hSSAO, the cavity seems smaller and is more occluded from bulk solvent. Although we have not observed any ability of TPP^+ to inhibit hSSAO activity, replacement of TPP^+ with the smaller mono-, di-, and tri-methylphenylphosphonium analogs also failed to cause any hSSAO inhibition, although potency versus BPAO was still evident (Supplemental Fig. S2). In the absence of an hSSAO inhibitor specifically targeting the secondary site, subsequent kinetic experiments focused upon compounds presumed to act primarily through binding to the active site, with the possibility that simultaneous binding of a second ligand molecule to the secondary site may also occur.

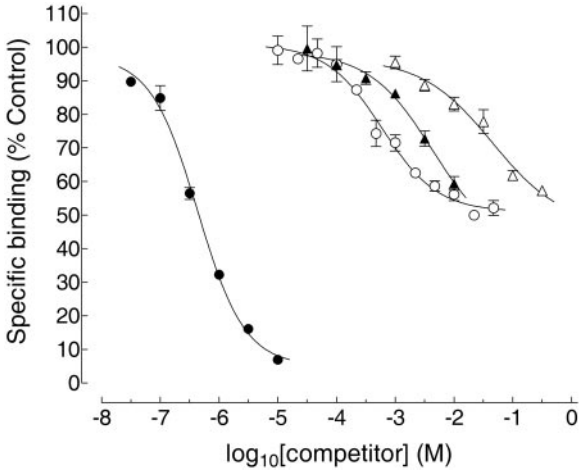

Fig. 3. Competition binding studies at the imidazoline binding site on BPAO. Specific binding of [^{3}H]TPP^+ (106 nM) to BPAO was assessed in the presence of TPP^+ (●), SPD (○), clonidine (▲), and BZ (△). Data were fitted to uniphasic sigmoidal curves with a four-parameter logistic equation. Although TPP^+ could displace all bound [^{3}H]TPP^+ in a uniphasic manner, SPD and BZ displaced approximately 49 and 59% at calculated plateaus, respectively, whereas curve fitting to clonidine data failed to indicate the position of a plateau. Competitor K_d values were calculated from IC_{50} values (see text). Issues relating to solubility and effects on nonspecific binding precluded the use of higher concentrations of competitor ligands. Data are the mean ± S.E.M. of three replicate determinations.

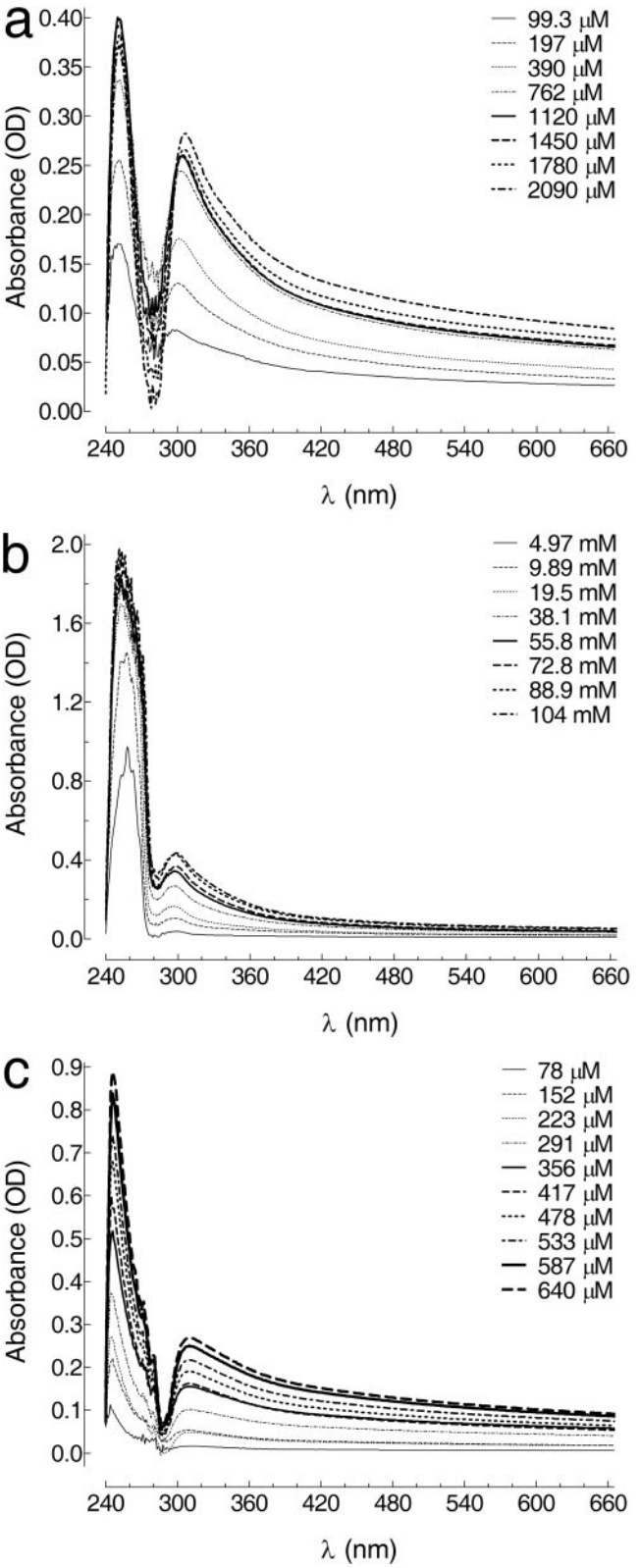

Fig. 4. BPAO difference spectra after anaerobic binding of SPD (a), BZ (b), and CLON (c) to the reduced enzyme. Ligands were added cumulatively to 10 μM BPAO, which had been reduced under anaerobic conditions with 50 μM BZ, and readings were recorded after spectra had stabilized (30 s–17 min).

Oxidation of all three hSSAO substrates examined (MA, BZ, and PEA) was regulated by each of the three reversible ligands used [GBZ, (+)TCP, and (+)AM] in a manner that could be accounted for adequately by the model shown in Scheme 1, described by eq. 2. Data obtained with GBZ are shown in Fig. 10, with kinetic constants obtained by global nonlinear regression listed in Table 2, along with those from experiments with (+)TCP and (+)AM.

We found no evidence supporting the view that any of the substrates or modulators examined interact with the secondary site on hSSAO in a manner that influences substrate kinetics. Accordingly, slight improvements in goodness-of-fit obtained with more complex kinetic models implicating binding at the secondary site (data not shown) were thought likely to be due to the increased number of variables and thus to the increased flexibility, in the associated equations.

Both the validity and the usefulness of the pseudoquantitative rapid equilibrium approach used to generate rate equations for reactions catalyzed by both BPAO and hSSAO are supported by the reproducibility of kinetic constants obtained by global analyses of data for a single substrate in the

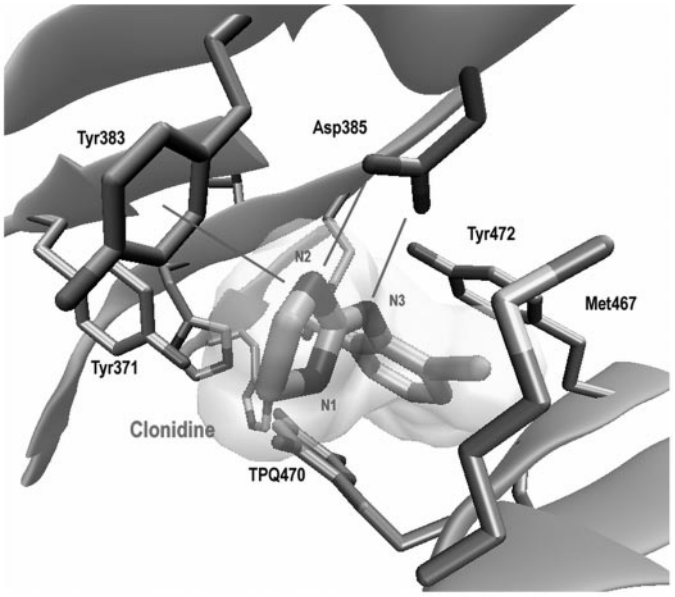

Fig. 5. Molecule of CLON bound within a BPAO active site. CLON occupies a hydrophobic pocket next to the Cu^{2+} binding site, forcing the cofactor (TPQ_{470}) into an on-copper inactive orientation. The aromatic ring of CLON is seen clearly to undergo π-stacking between the rings of TPQ_{470} and Tyr_{472}. Hydrogen bonding of CLON nitrogens N2 and N3 to Tyr_{383} and Asp_{385} are indicated by hatched lines.

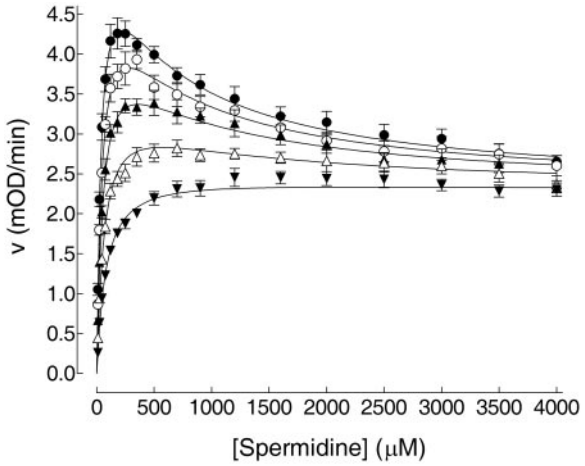

Fig. 6. Effects of TPP^+ on oxidation of SPD by BPAO. SPD (10 μM–4 mM) was incubated with BPAO in the absence (controls; ●) or presence of TPP^+ at concentrations of 50 (○), 120 (▲), 250 (△), and 500 nM (▼). Initial velocities were measured by a peroxidase-coupled absorbance assay. Data were fitted with eq. 2 by the global curve-fitting nonlinear regression facility of GraphPad Prism version 5.00. Kinetic constants thereby derived are listed in Table 1. Data are the mean ± S.E.M. of five replicate observations.

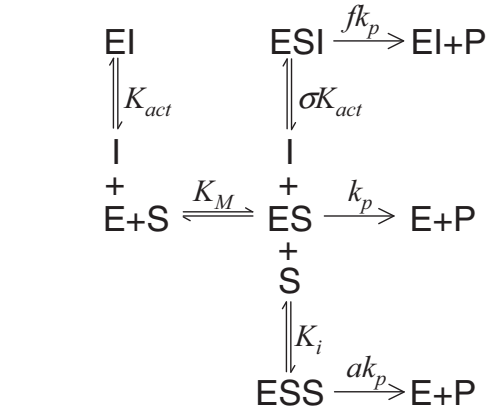

Scheme 1. Reaction scheme for interactions of a single substrate molecule or a single inhibitor molecule with the active site on oxidized and reduced SSAO enzyme forms. To facilitate equation derivation by a pseudoquantitative rapid equilibrium approach (see text), ES is used to refer both to oxidized enzyme with substrate bound and to reduced enzyme after release of aldehyde product. As such, when substrate or inhibitor binds to the reduced enzyme, the resulting species are indicated as ESS or ESI, respectively. The equation describing this mechanism is eq. 2. If binding of substrate and inhibitor are exclusive processes, the value of factor f should approximate zero. Although scheme 1 (and eq. 2) illustrates interactions of substrate and inhibitor with the SSAO active site, binding of an exclusive imidazoline site-directed BPAO inhibitor, such as TPP^+, and subsequent competitive inhibition of oxidation of a bridging substrate such as SPD, may also be described by this scheme if K_{act}, σ, and f are replaced with K_{imid}, γ, and d, respectively (see text).

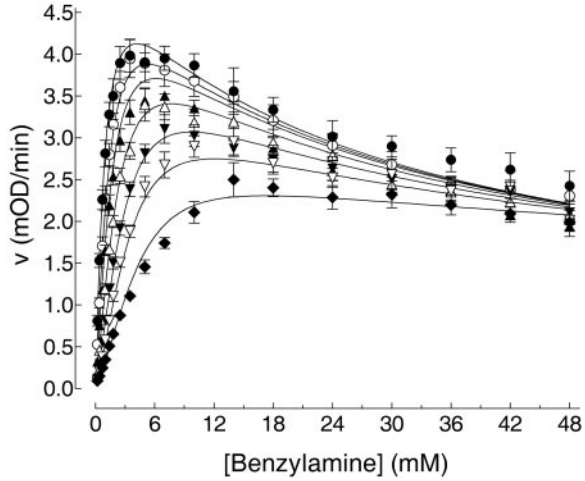

Fig. 7. Effects of TPP^+ on oxidation of BZ by BPAO. BZ (200 μM–48 mM) was incubated with BPAO in the absence (controls; ●) or presence of TPP^+ at concentrations of 150 nM (○), 300 nM (▲), 700 nM (△), 1.5 μM (▼), 3 μM (▽), and 10 μM (♦). Initial velocities were measured by a peroxidase-coupled absorbance assay. Data were fitted with Supplemental Eq. S1 by the global curve-fitting nonlinear regression facility of GraphPad Prism version 5.00. Kinetic constants thereby derived are listed in Supplemental Table S2. Data are the mean ± S.E.M. of four replicate observations.

presence of different modulators (mean ± S.E. values in Tables 1 and 2 and Supplemental Table S2).

The combinations of enzyme-ligand interactions proposed to occur based on results from the kinetic, spectral, radioligand binding and crystallographic studies described here are illustrated in Fig. 11.

Discussion

We have examined interactions of substrates and modulators with BPAO, an enzyme for which extensive structural and mechanistic data are available (Janes et al., 1990; Hartmann et al., 1993; Su and Klinman, 1998; Lunelli et al., 2005), and which has been purified in amounts sufficient to facilitate spectroscopic and radioligand binding studies. Kinetic models based upon information obtained from experiments with BPAO were applied to recombinant hSSAO, available in amounts precluding spectroscopic analyses, to define the roles played by substrates and modulators binding to active and imidazoline binding sites in regulating substrate catalysis.

Extended kinetic curves for copper-containing amine oxidases show clearly that initial velocities fall at higher substrate concentrations (McEwen, 1965; Ignesti, 2003; Shepard and Dooley, 2006; Holt et al., 2007). With both BPAO and hSSAO, oxidation proceeds by a ping-pong bi-ter process. Although methodologies are available that could generate substrate inhibition equations in such systems, these involve complex mathematics (Bardsley et al., 1980; Segel, 1993) that become unmanageable when terms describing regulators acting at multiple sites are introduced.

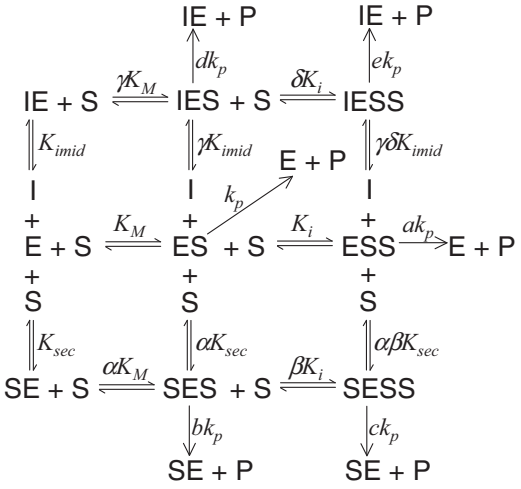

Scheme 2. Reaction scheme for interactions of small substrate molecule(s) with active and/or secondary (imidazoline) sites, and interactions of a single molecule of TPP^+ with the secondary site, on oxidized and reduced SSAO enzyme forms. The equation describing this mechanism is Supplemental eq. S1. Notations used are as indicated in the legends to Scheme 1 and Table 1. In addition, binding of a ligand to the SSAO active site is indicated by inclusion of a suffix to E, whereas binding to the secondary site is indicated by inclusion of a prefix to E. For example, IESS refers to reduced SSAO (ES) with a single substrate molecule (suffix S) bound to the active site and TPP^+ (prefix I) bound to the secondary site.

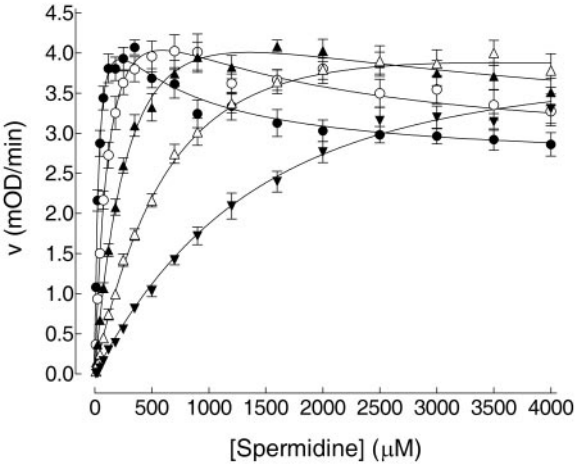

Fig. 8. Effects of CLON on oxidation of SPD by BPAO. SPD (10 μM–4 mM) was incubated with BPAO in the absence (controls; ●) or presence of CLON at concentrations of 50 μM (○), 150 μM (▲), 400 μM (△), and 1 mM (▼). Initial velocities were measured by a peroxidase-coupled absorbance assay. Data were fitted with Supplemental Eq. S2 by the global curve-fitting nonlinear regression facility of GraphPad Prism version 5.00. Kinetic constants thereby derived are listed in Table 1. Data are the mean ± S.E.M. of five replicate observations.

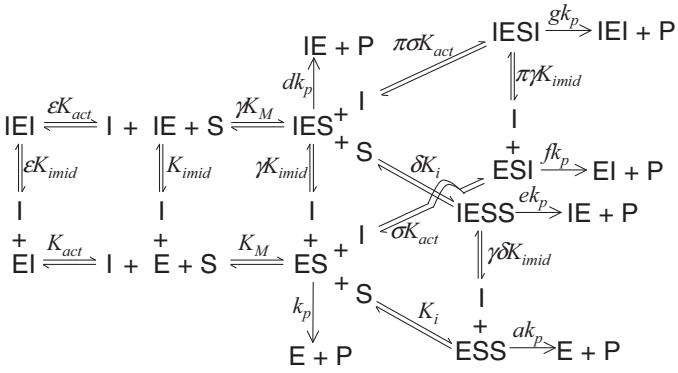

Scheme 3. Reaction scheme for interactions of a single substrate molecule with the active site, and interactions of inhibitor/modulator molecule(s) with the active and/or secondary sites, on oxidized and reduced SSAO enzyme forms. Supplemental Equation S2 describes this mechanism. Notations used are as indicated in the legends to Schemes 1 and 2.

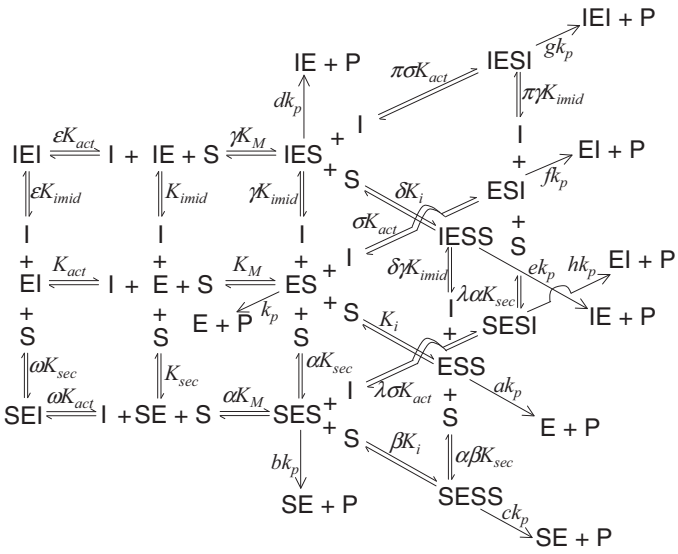

Scheme 4. Reaction scheme for interactions of small substrate molecule(s) with the active and/or secondary sites, and interactions of inhibitor/modulator molecule(s) with the active and/or secondary sites, on oxidized and reduced SSAO enzyme forms. Supplemental Equation S3 describes this mechanism. Notations used are as indicated in the legends to Schemes 1 and 2.

We therefore adopted a pseudoquantitative rapid equilibrium approach, in which several intermediate reactions are grouped together under one pseudo rate constant. In designating ES to represent both E_{ox}-NH^+CH_2R and E_{red}, we imply the existence of only one enzyme species (E), with formation of Schiff's base intermediates, release of aldehyde, and generation of an aminoquinol (Mure et al., 2002), occurring instantaneously. The rate-limiting contribution of this reductive half-reaction (Farnum et al., 1986) indicates that this implication is incorrect. We have nevertheless found these equations useful for fitting multiple data sets with the global nonlinear regression facility of GraphPad Prism, because acceptable global fits are generally obtained only when underlying models are correct.

Subsequently, we have found that oxidation of SPD by BPAO is consistent with a model describing partial uncompetitive inhibition by substrate (Holt et al., 2007). Although kinetic analyses could also be interpreted as substrate binding to a separate allosteric site, or as cooperativity between subunits, spectroscopic data support the view that substrates can bind both to the active site of resting enzyme and to the aminoquinol (reduced) active site after release of aldehyde. Addition of BZ to anaerobic BPAO resulted in characteristic absorbance changes, with peaks at 300 to 310 nm and 480 nm associated with reduced TPQ cofactor (Hartmann et al., 1993). Addition of SPD to reduced BPAO resulted in a concentration-dependent increase in the 300- to 310-nm peak height, suggesting that SPD binds sufficiently close to reduced TPQ to cause perturbation of the cofactor absorbance spectrum.

With this two-site model used to describe oxidation of BZ by BPAO, addition of steps to account for effects of CLON and other modulators on BZ metabolism were unsuccessful. Previous kinetic analyses indicated that CLON and other imidazoline ligands bind to four sites on BPAO (Holt et al., 2004). Therefore, we hypothesized that two of these sites correspond to the active site on an oxidized and reduced

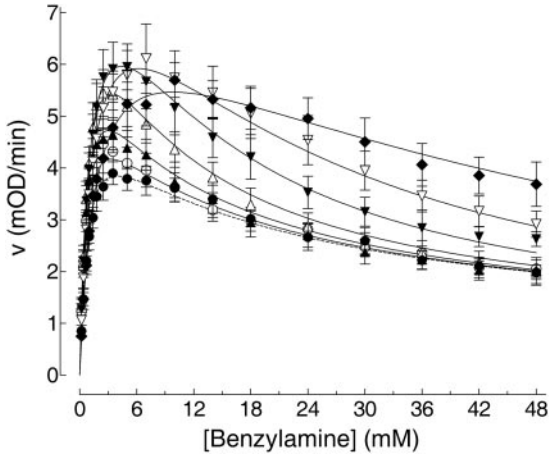

Fig. 9. Effects of CLON on oxidation of BZ by BPAO. BZ (200 μM–48 mM) was incubated with BPAO in the absence (controls; ●) or presence of CLON at concentrations of 30 μM (○), 100 μM (▲), 300 μM (△), 1 mM (▼), 3 mM (▽), and 10 mM (◆). Initial velocities were measured by a peroxidase-coupled absorbance assay. Data were fitted with Supplemental Eq. S3 by the global curve-fitting nonlinear regression facility of GraphPad Prism version 5.00. Kinetic constants thereby derived are listed in Supplemental Table S2. The curve fitted to control data are shown as a hatched line to emphasize the stimulatory effects of CLON with BZ as substrate. Data are the mean ± S.E.M. of four replicate observations.

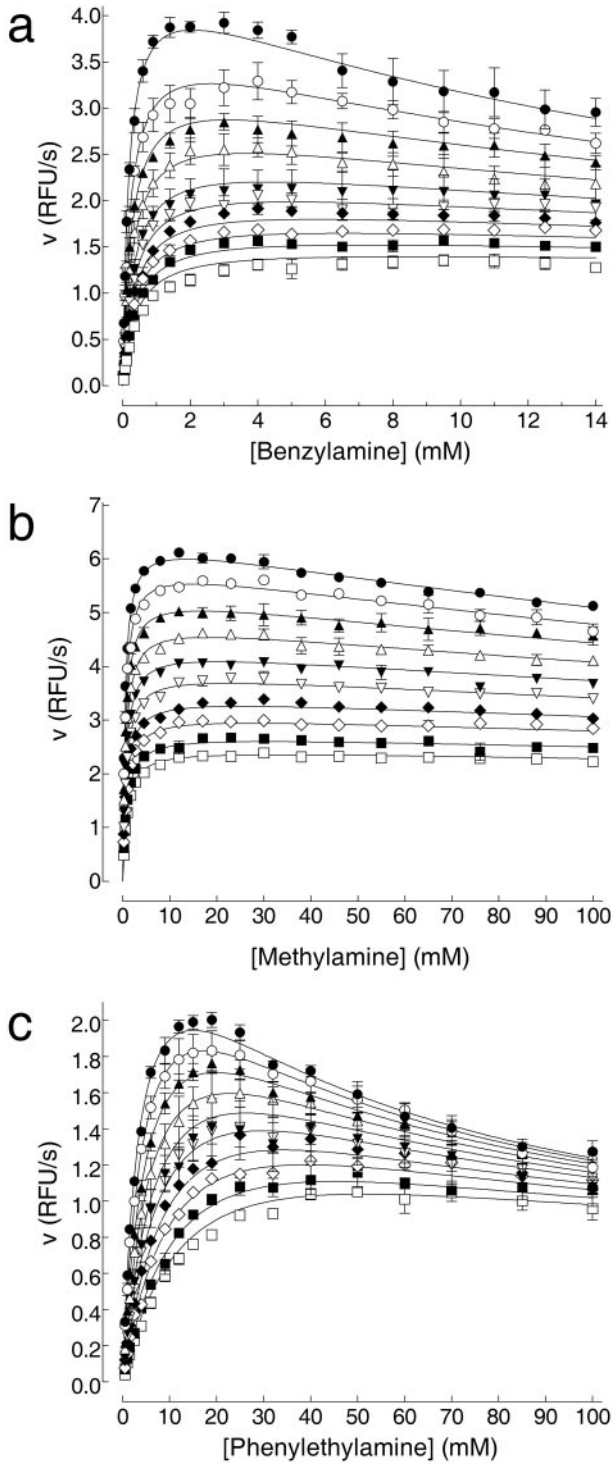

Fig. 10. Effects of GBZ on oxidation of BZ (a), MA (b), and PEA (c) by hSSAO. Substrates (BZ, 30 μM–14 mM; MA, 250 μM–100 mM; PEA, 500 μM–100 mM) were incubated with hSSAO in the absence (controls; ●) or presence of GBZ at concentrations of 6 (○), 12 (▲), 20 (△), 30 (▼), 40 (▽), 52 (◆), 65 (◇), 80 (■), and 100 μM (□) (with BZ as substrate) or at concentrations of 3 (○), 7 (▲), 12 (△), 18 (▼), 25 (▽), 35 (◆), 45 (◇), 60 (■), and 75 μM (□) (with MA or PEA as substrate). Initial velocities were measured by a peroxidase-coupled fluorescence assay. Data were fitted with eq. 2 by the global curve-fitting nonlinear regression facility of GraphPad Prism version 5.00. Kinetic constants thereby derived are listed in Table 2. Data are the mean ± S.E.M. of three replicate observations.

subunit and that the remaining two sites correspond to the TPP^+/imidazoline site present on an oxidized and reduced subunit. Through use of a novel radioligand binding assay procedure allowing quantification of modest affinity binding of $[^3H]TPP^+$ to pure soluble BPAO, we found that CLON, and SPD and BZ, could compete with $[^3H]TPP^+$ for specific binding. Furthermore, although examination of BPAO crystals grown in the presence of CLON did not reveal low-affinity binding at the imidazoline site, marked distortion of residues Glu_{432}-Val_{458}, at the mouth of the substrate entrance channel and within the hairpin loop region, was nevertheless apparent. Significantly, binding of CLON was confirmed within the active site cavity, with the aromatic ring of CLON π-stacked between the rings of TPQ_{470} and Tyr_{472}, forcing the TPQ into an inactive on-copper conformation. Taken together, these data indicate that although compounds such as SPD are able to bridge the active and imidazoline sites of BPAO, smaller cationic species such as BZ or CLON may bind at one or both of the active and imidazoline sites on both an oxidized and a reduced subunit.

Accordingly, control BZ data were fitted to a model allowing BZ to bind to the active and imidazoline sites on BPAO, binding to the latter influencing substrate access and/or substrate kinetics at the active site, to some degree. Nevertheless, inhibition remained partial for both BZ and SPD, suggesting that enzyme can still be reoxidized in the presence of substrate at a concentration sufficient to saturate the reduced active site, albeit at a rate lower than that at which

TABLE 2

Kinetic constants determined for metabolism of amines by hSSAO in the presence of modulatory ligands, measured in a fluorescence assay

Data were obtained from global nonlinear regression of 10 data sets (curves) composed of 18 points per curve, with three replicate determinations made for each point. Other details are as indicated for Table 1.

Modulator	Eq. No.	V_{max}	K_M	K_i	K_{act}	σ	a	f	r^2	n
		RFU/s		*mM*						
BZ as substrate										
Control	PUS	4.769 (0.385)	0.194 (0.043)	11.5 (14.7)			0.3311 (0.3623)		0.8251	3
(+)TCP	2	5.395 (0.054)	0.162 (0.006)	19.3 (4.303)	0.731 (0.044)	17.7 (2.9)	0.283 (0.084)	≈0	0.982	3
GBZ	2	4.529 (0.086)	0.184 (0.011)	18.7 (3.9)	0.011 (0.001)	2.41 (0.29)	0.166 (0.075)	0.154 (0.013)	0.970	3
(+)AM	2	4.073 (0.103)	0.181 (0.013)	13.1 (3.7)	17.1 (27.3)	0.121 (0.200)	0.260 (0.077)	≈0	0.899	3
Mean ± S.E.			0.180 ± 0.007	15.7 ± 2.0			0.260 ± 0.035			
MA as substrate										
Control	PUS	5.691 (0.418)	0.576 (0.166)	237 (+)			0.294 (+)		0.584	3
(+)TCP	2	6.599 (0.043)	0.458 (0.016)	406 (41)	0.542 (0.053)	24.0 (17.1)	≈0	≈0	0.973	3
GBZ	2	6.400 (0.031)	0.461 (0.011)	398 (27)	0.0142 (0.0006)	2.14 (0.11)	≈0	0.136 (0.008)	0.992	3
(+)AM	2	4.599 (0.048)	0.642 (0.024)	96.1 (11.9)	4.93 (2.12)	0.255 (0.102)	0.515 (0.018)	0.015 (0.053)	0.966	3
Mean ± S.E.			0.534 ± 0.045	284 ± 74			0.202 ± 0.125			
PEA as substrate										
Control	PUS	2.741 (0.370)	3.78 (1.09)	70.8 (73.4)			0.040 (+)		0.8035	3
(+)TCP	2	3.157 (0.067)	3.45 (0.18)	63.8 (8.2)	0.564 (0.035)	5.07 (0.65)	0.116 (0.033)	≈0	0.980	3
GBZ	2	2.928 (0.119)	3.81 (0.336)	43.7 (8.4)	0.011 (0.001)	5.94 (1.32)	0.178 (0.033)	0.157 (0.047)	0.961	3
(+)AM	2	2.405 (0.116)	4.54 (0.42)	39.7 (7.7)	3.68 (1.35)	0.710 (0.333)	0.127 (0.037)	0.377 (0.089)	0.922	3
Mean ± S.E.			3.90 ± 0.23	54.5 ± 7.6			0.115 ± 0.028			

RFU, relative fluorescent units.

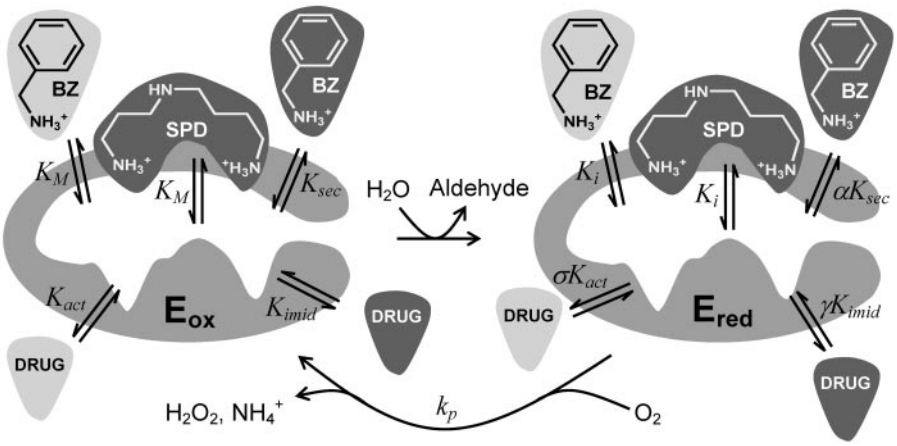

Fig. 11. Cartoon illustrating the catalytic cycles of BPAO and hSSAO and the combinations of ligand-protein equilibria affecting reaction velocities. Enzymes contain anionic cavities close to the mouth of the entrance channel (the imidazoline site) or deep within the protein (the active site). Molecules shown as light structures on a dark background reflect binding only to BPAO and not to hSSAO. Substrates may bind to the active site on the oxidized (K_M) or reduced (K_i) enzyme forms. Binding of SPD bridges both the active and imidazoline sites of BPAO; in contrast, binding of smaller substrates such as BZ to the active site does not preclude binding of a second substrate molecule to the imidazoline site on the oxidized (K_{sec}) or reduced (αK_{sec}) forms of BPAO. Drug ligands may compete with substrates for binding to the active site on the oxidized (K_{act}) and reduced (σK_{act}) enzymes, and/or in the case of BPAO, for binding to the imidazoline site on the oxidized (K_{imid}) and reduced (γK_{imid}) forms of BPAO. Binding of substrates to the active site of the oxidized enzyme results in catalysis, whereas binding to the active site of the reduced enzyme results in substrate inhibition. The specific effects of a modulator on enzyme activity depend largely upon the relative degrees to which catalysis and substrate inhibition are influenced by the compound of interest. Although the current kinetic studies revealed no requirement for involvement of an imidazoline binding site on hSSAO to model data successfully, the potential nevertheless exists for future noncompetitive hSSAO inhibitors to target this anionic cavity, and novel hSSAO ligands that bind solely, or in a bridging manner, to the imidazoline site may offer significant improvements in selectivity, potency, and side effect profile.

enzyme reoxidation normally occurs. It seems unlikely that substrate binds directly to the reduced cofactor. Rather, electrostatic and hydrophobic interactions, including aromatic stacking similar to that observed with CLON, may facilitate substrate binding within the reduced active site. Binding of substrate in this manner may result in steric hindrance of O_2 access to, or of H_2O_2 diffusion from, the active site copper-quinone complex, thereby reducing catalytic rate constants. Such a mechanism may be supported by the observation that binding of CLON to BPAO resulted in some displacement of residues forming a channel from the large internal cavity of the dimer via which O_2 and H_2O_2 may enter and exit the active site (Lunelli et al., 2005). Alternatively, it is also possible that substrate binding stabilizes the aminoquinol enzyme in a nonproductive on-copper conformation.

Our analyses support the view that activation of BPAO by imidazoline ligands results from disinhibition of the enzyme by competition with substrate for binding to E_{red}, leading to a drug-E_{red} complex which reoxidizes more rapidly than a substrate-E_{red} complex, and an apparent reduction in K_M typical of an ordered uncompetitive mechanism (Segel, 1993). The substrate dependence of modulation may thus be attributed to the relative affinities of the substrate and modulator for both enzyme forms and to the relative rates of reoxidation of the complexes formed between E_{red} and the respective ligands. Enzyme activation with CLON, for example, may then reflect a faster off-rate for CLON, compared with that for substrate, with reoxidation occurring while dissociated CLON occludes the substrate entrance channel. It is interesting that substrate inhibition is attenuated as the concentration of buffer cations increases (Holt et al., 2007). Alkali metal cations may bind close to an on-copper iminoquinone in *Hansenula polymorpha* copper amine oxidase (Plastino et al., 1999), and it seems plausible that cation binding close to an aminoquinol may repel binding of cationic substrate without hindering enzyme reoxidation.

Kinetic analyses of the effects of several reversible BPAO modulators support binding of ligands to both the active and imidazoline sites on oxidized and reduced BPAO, with modulation occurring in a substrate-specific manner. Although CLON enhanced SPD oxidation only at high substrate concentrations, BZ oxidation was always enhanced, relative to controls. GBZ and (+)TCP caused only inhibition at all substrate concentrations. BZ oxidation was always inhibited by 2-BFI, whereas SPD metabolism was enhanced at higher substrate concentrations. Effects versus SPD occurred at 2-BFI concentrations 10-fold lower than those versus BZ, indicating a preference for binding of 2-BFI to the imidazoline site. TPP^+, which only binds to the imidazoline site, was far more potent as an inhibitor of SPD oxidation, consistent with previous observations (Di Paolo et al., 2004).

When mechanisms deduced for BPAO were applied to kinetic data for hSSAO, curves could be fitted successfully with two-site equations describing ligands binding only at the active site, even in the case of ligands that bound to both active and imidazoline sites on BPAO. SPD is neither a substrate nor a competitive inhibitor of hSSAO (A. Holt, unpublished data), perhaps because the Leu_{469} active site gate (Airenne et al., 2005) would require SPD to adopt a sharply angled conformation to bind. Although an hSSAO substrate that bridges the active and imidazoline sites is not presently available, neither TPP^+ nor its analogs were able to inhibit turnover of the smaller amine substrates used, and binding of TPP^+ analogs to the imidazoline site on hSSAO without affecting enzyme activity cannot be ruled out.

Although none of the compounds tested enhanced substrate turnover, substrate inhibition of hSSAO was nevertheless evident, and it is presumed that the mechanism by which this occurs is similar to that with BPAO. Thus, enhancement of hSSAO activity by a suitable modulator seems feasible. In this regard, an endogenous substrate such as methylamine might either inhibit or enhance the oxidation of other substrates, including protein-bound substrates, thereby offering a novel mechanism for regulating the physiological function of hSSAO. Furthermore, the substrate selectivity that is clearly evident for inhibitors/modulators of hSSAO (and BPAO) may offer therapeutic benefits, because physiological and pathophysiological roles for hSSAO may involve several distinct substrates. Thus, it may be possible to inhibit a deleterious action of hSSAO while leaving physiological functioning of the enzyme largely unaltered.

Our data thus offer a feasible explanation for several anomalous kinetic observations made previously with copper-containing amine oxidases. Drugs that show selectivity for oxidized or reduced hSSAO, or that bridge active and imidazoline sites, may possess unique therapeutic potential as regulators of hSSAO in inflammatory cardiovascular conditions.

Acknowledgments

We thank Owen Degenhardt for technical assistance. We are grateful to Drs. David Dooley, Eric Shepard, Keith Tipton, and Irwin Segel for helpful discussions.

References

Airenne TT, Nymalm Y, Kidron H, Smith DJ, Pihlavisto M, Salmi M, Jalkanen S, Johnson MS, and Salminen TA (2005) Crystal structure of the human vascular adhesion protein-1: unique structural features with functional implications. *Protein Sci* **14:**1964–1974.

Bardsley WG, Leff P, Kavanagh J, and Waight RD (1980) Deviations from Michaelis-Menten kinetics. The possibility of complicated curves for simple kinetic schemes and the computer fitting of experimental data for acetylcholinesterase, acid phosphatase, adenosine deaminase, arylsulphatase, benzylamine oxidase, chymotrypsin, fumarase, galactose dehydrogenase, beta-galactosidase, lactate dehydrogenase, peroxidase and xanthine oxidase. *Biochem J* **187:**739–765.

Boomsma F, Hut H, Bagghoe U, van der Houwen A, and van den Meiracker A (2005) Semicarbazide-sensitive amine oxidase (SSAO): from cell to circulation. *Med Sci Monit* **11:**RA122–RA126.

Calderone V, Di Paolo ML, Trabucco M, Biadene M, Battistutta R, Rigo A, and Zanotti G (2003) Crystallization and preliminary X-ray data of amine oxidase from bovine serum. *Acta Crystallogr D Biol Crystallogr* **59:**727–729.

Carpéné C, Collon P, Remaury A, Cordi A, Hudson A, Nutt D, and Lafontan M (1995) Inhibition of amine oxidase activity by derivatives that recognize imidazoline I2 sites. *J Pharmacol Exp Ther* **272:**681–688.

Di Paolo ML, Lunelli M, Scarpa M, and Rigo A (2004) Phosphonium compounds as new and specific inhibitors of bovine serum amine oxidase. *Biochem J* **384:**551–558.

Di Paolo ML, Pesce C, Lunelli M, Scarpa M, and Rigo A (2007) N-Alkanamines as substrates to probe the hydrophobic region of bovine serum amine oxidase active site: a kinetic and spectroscopic study. *Arch Biochem Biophys* **465:**50–60.

Di Paolo ML, Stevanato R, Corazza A, Vianello F, Lunelli L, Scarpa M, and Rigo A (2003) Electrostatic compared with hydrophobic interactions between bovine serum amine oxidase and its substrates. *Biochem J* **371:**549–556.

Farnum M, Palcic MM, and Klinman JP (1986) pH Dependence of deuterium isotope effects and tritium exchange in the bovine plasma amine oxidase reaction: a role for single-base catalysis in amine oxidation and imine exchange. *Biochemistry* **25:**1898–1904.

Gubisne-Haberle D, Hill W, Kazachkov M, Richardson JS, and Yu PH (2004) Protein cross-linkage induced by formaldehyde derived from semicarbazide-sensitive amine oxidase-mediated deamination of methylamine. *J Pharmacol Exp Ther* **310:**1125–1132.

Hartmann C, Brzovic P, and Klinman JP (1993) Spectroscopic detection of chemical intermediates in the reaction of para-substituted benzylamines with bovine serum amine oxidase. *Biochemistry* **32:**2234–2241.

Head GA and Mayorov DN (2006) Imidazoline receptors, novel agents and therapeutic potential. *Cardiovasc Hematol Agents Med Chem* **4:**17–32.

Holt A, Alton G, Scaman C, Loppnow GR, Szpacenko A, Svendsen I, and Palcic MM

(1998) Identification of the quinone cofactor in mammalian semicarbazide-sensitive amine oxidase. *Biochemistry* **37:**4946–4957.
Holt A, Degenhardt OS, Berry PD, Kapty JS, Mithani S, Smith DJ, and Di Paolo ML (2007) The effects of buffer cations on interactions between mammalian copper-containing amine oxidases and their substrates. *J Neural Transm* **114:**733–741.
Holt A and Palcic MM (2006) A peroxidase-coupled continuous absorbance plate-reader assay for flavin monoamine oxidases, copper-containing amine oxidases and related enzymes. *Nature Protocols* **1:**2498–2505.
Holt A, Wieland B, and Baker GB (2004) Allosteric modulation of semicarbazide-sensitive amine oxidase activities in vitro by imidazoline receptor ligands. *Br J Pharmacol* **143:**495–507.
Ignesti G (2003) Equations of substrate-inhibition kinetics applied to pig kidney diamine oxidase (DAO, E.C. 1.4.3.6). *J Enzyme Inhib Med Chem* **18:**463–473.
Jalkanen S, Karikoski M, Mercier N, Koskinen K, Henttinen T, Elima K, Salmivirta K, and Salmi M (2007) The oxidase activity of vascular adhesion protein-1 (VAP-1) induces endothelial E- and P-selectins and leukocyte binding. *Blood* **110:**1864–1870.
Janes SM, Mu D, Wemmer D, Smith AJ, Kaur S, Maltby D, Burlingame AL, and Klinman JP (1990) A new redox cofactor in eukaryotic enzymes: 6-hydroxydopa at the active site of bovine serum amine oxidase. *Science* **248:**981–987.
Leslie AGW (1992) Recent changes to the MOSFLM package for processing film and image plate data, in *Joint CCP4 and ESF-EAMCB Newsletter on Protein Crystallography, No. 26*, Daresbury Laboratory, Warrington, UK.
Lunelli M, Di Paolo ML, Biadene M, Calderone V, Battistutta R, Scarpa M, Rigo A, and Zanotti G (2005) Crystal structure of amine oxidase from bovine serum. *J Mol Biol* **346:**991–1004.
Lyles GA (1984) The interaction of semicarbazide-sensitive amine oxidase with MAO inhibitors, in *Monoamine Oxidase and Disease* (Tipton KF, Dostert P, and Strolin Benedetti M eds) pp 547–556, Academic Press, London, UK.
Lyles GA (1995) Substrate-specificity of mammalian tissue-bound semicarbazide-sensitive amine oxidase. *Prog Brain Res* **106:**293–303.
McEwen CM Jr (1965) Human plasma monoamine oxidase. II. Kinetic studies. *J Biol Chem* **240:**2011–2018.
Menguy T, Chenevois S, Guillain F, le Maire M, Falson P, and Champeil P (1998) Ligand binding to macromolecules or micelles: use of centrifugal ultrafiltration to measure low-affinity binding. *Anal Biochem* **264:**141–148.
Morpurgo L, Agostinelli E, Mondovi B, Avigliano L, Silvestri R, Stefancich G, and Artico M (1992) Bovine serum amine oxidase: half-site reactivity with phenylhydrazine, semicarbazide, and aromatic hydrazides. *Biochemistry* **31:**2615–2621.
Mure M, Mills SA, and Klinman JP (2002) Catalytic mechanism of the topa quinone containing copper amine oxidases. *Biochemistry* **41:**9269–9278.
Murshudov GN, Vagin AA, and Dodson EJ (1997) Refinement of macromolecular structures by the maximum-likelihood method. *Acta Crystallogr D Biol Crystallogr* **53:**240–255.
Ozaita A, Olmos G, Boronat MA, Lizcano JM, Unzeta M, and Garcia-Sevilla JA (1997) Inhibition of monoamine oxidase A and B activities by imidazol(ine)/guanidine drugs, nature of the interaction and distinction from I2-imidazoline receptors in rat liver. *Br J Pharmacol* **121:**901–912.
Plastino J, Green EL, Sanders-Loehr J, and Klinman JP (1999) An unexpected role for the active site base in cofactor orientation and flexibility in the copper amine oxidase from *Hansenula polymorpha*. *Biochemistry* **38:**8204–8216.
Remko M, Walsh OA, and Richards WG (2001) Molecular structure and gas-phase reactivity of clonidine and rilmenidine: two-layered ONIOM calculations. *Phys Chem Chem Phys* **3:**901–907.
Salmi M and Jalkanen S (2001) VAP-1: an adhesin and an enzyme. *Trends Immunol* **22:**211–216.
Sayre LM, Naismith RT, 2nd, Bada MA, Li WS, Klein ME, and Tennant MD (1996) trans-2-Phenylcyclopropylamine is a substrate for and inactivator of horseradish peroxidase. *Biochim Biophys Acta* **1296:**250–256.
Schüttelkopf AW and van Aalten DM (2004) PRODRG: a tool for high-throughput crystallography of protein-ligand complexes. *Acta Crystallogr D Biol Crystallogr* **60:**1355–1363.
Schwelberger HG (2007) The origin of mammalian plasma amine oxidases. *J Neural Transm* **114:**757–762.
Segel IH (1993) *Enzyme Kinetics. Behavior and Analysis of Rapid Equilibrium and Steady-State Enzyme Systems*, John Wiley & Sons, Inc., New York.
Sheldrick GM and Schneider TR (1997) SHELXL: high resolution refinement, in *Methods in Enzymology* (Carter CWJ and Sweet RM eds) pp 319–343, Academic Press, San Diego, CA.
Shepard EM and Dooley DM (2006) Intramolecular electron transfer rate between active-site copper and TPQ in *Arthrobacter globiformis* amine oxidase. *J Biol Inorg Chem* **11:**1039–1048.
Su Q and Klinman JP (1998) Probing the mechanism of proton coupled electron transfer to dioxygen: the oxidative half reaction of bovine serum amine oxidase. *Biochemistry* **37:**12513–12525.
Wang EY, Gao H, Salter-Cid L, Zhang J, Huang L, Podar EM, Miller A, Zhao J, O'Rourke A, and Linnik MD (2006) Design, synthesis, and biological evaluation of semicarbazide-sensitive amine oxidase (SSAO) inhibitors with anti-inflammatory activity. *J Med Chem* **49:**2166–2173.

Address correspondence to: Dr. Andrew Holt, Department of Pharmacology, Faculty of Medicine and Dentistry, 9-70 Medical Sciences Bldg., University of Alberta, Edmonton, AB, Canada, T6G 2H7. E-mail: aholt@pmcol.ualberta.ca